atoms

MDPI

Article

Quasars: From the Physics of Line Formation to Cosmology

Paola Marziani [1,*], Edi Bon [2], Natasa Bon [2], Ascension del Olmo [3], Mary Loli Martínez-Aldama [3], Mauro D'Onofrio [4], Deborah Dultzin [5], C. Alenka Negrete [5] and Giovanna M. Stirpe [6]

1 National Institute for Astrophysics (INAF), Astronomical Observatory of Padova, IT-35122 Padova, Italy
2 Astronomical Observatory, 11060 Belgrade, Serbia; ebon@aob.rs (E.B.); nbon@aob.rs (N.B.)
3 Instituto de Astrofisíca de Andalucía, IAA-CSIC, Glorieta de la Astronomia s/n, E-18008 Granada, Spain; chony@iaa.es (A.d.O.); mmary@cft.edu.pl (M.L.M.-A.)
4 Dipartimento di Fisica & Astronomia "Galileo Galilei", Università di Padova, IT-35122 Padova, Italy; Mauro.donofrio@unipd.it
5 Instituto de Astronomía, UNAM, Mexico D.F. 04510, Mexico; deborah@astro.unam.mx (D.D.); negrete@astro.unam.mx (C.A.N.)
6 INAF, Osservatorio di Astrofisica e Scienza dello Spazio, IT-40129 Bologna, Italy; giovanna.stirpe@inaf.it
* Correspondence: paola.marziani@inaf.it; Tel.: +39-0498293415

Received: 26 November 2018; Accepted: 28 January 2019; Published: 4 February 2019

Abstract: Quasars accreting matter at very high rates (known as extreme Population A (xA) or super-Eddington accreting massive black holes) provide a new class of distance indicators covering cosmic epochs from the present-day Universe up to less than 1 Gyr from the Big Bang. The very high accretion rate makes it possible that massive black holes hosted in xA quasars can radiate at a stable, extreme luminosity-to-mass ratio. This in turn translates into stable physical and dynamical conditions of the mildly ionized gas in the quasar low-ionization line emitting region. In this contribution, we analyze the main optical and UV spectral properties of extreme Population A quasars that make them easily identifiable in large spectroscopic surveys at low- ($z \lesssim 1$) and intermediate-z ($2 \lesssim z \lesssim 2.6$), and the physical conditions that are derived for the formation of their emission lines. Ultimately, the analysis supports the possibility of identifying a virial broadening estimator from low-ionization line widths, and the conceptual validity of the redshift-independent luminosity estimates based on virial broadening for a known luminosity-to-mass ratio.

Keywords: black hole physics; cosmology; quasar spectroscopy; cosmological parameters; ionized gas; broad line region

1. Introduction

1.1. Quasar Spectra: Emission from Mildly Ionized Gas

The spectra of quasars can be easily recognized by the presence of broad and narrow optical and UV lines emitted by mildly-ionized species over a wide range of ionization potential. The type-1 composite quasar spectrum from the Sloan Digital Sky Survey (SDSS) [1] reveals Broad (FWHM $\gtrsim$ 1000 km s^{-1}) and Narrow High Ionization lines (HILs, 50 eV) and Low Ionization lines (LILs, <20 eV). Broad HILs encompass CIVλ1549, HeIIλ1640 and HeIIλ4686 as representative specimens. Broad LILs include HI Balmer lines (Hβ, Hα), MgIIλ2800, the CaII IR Triplet, and FeII features. The FeII emission deserves a particular mention, as it is extended over a broad range of wavelengths (Figure 6 of [2]), and is especially prominent around MgIIλ2800 and Hβ. The FeII emission is one of the dominant coolants in the broad line region (BLR) and therefore a main factor in its energetic balance (the FeII emission extends from the UV to the far IR, and can reach the luminosity of Lyα, [3,4]). Thus, it may not appear surprising that an estimator of its strength plays an important role in the systematic organization of quasar properties (Section 2).

This paper reviews results obtained in the course of two decades (Sections 2 and 3), attempting to explain how the spectral properties of a class of type-1 quasars and their physical interpretation can lead to the definition of "Eddington standard candles" (ESC, Section 4). In the following, we will restrict the presentation to type-1 quasars which are considered mainly "unobscured" sources with an unimpeded view of the BLR, and exclude type-2 active galactic nuclei (AGN) or quasars in which the broad lines are not detected in natural light (see [5] for an exhaustive review). We describe the physical basis of the method in Sections 3 and 4. We then introduce ESC selection criteria (Section 5) and preliminary cosmology results (Section 6).

1.2. Quasars for Cosmology: An Open Issue

The distribution of quasars in space and the intervening absorptions along the line of sight (i.e., the so called Lyα forest) has long been considered as a tracer of matter in the distant Universe (see [6] and references therein). However, a relevant question may be why intrinsic properties of quasars have never been successfully used as cosmological probes. On the one hand, (1) quasars are easily recognizable and plentiful ($\gtrsim$500,000 in the data release 14 of the SDSS, [7]). (2) They are very luminous and can reach bolometric luminosity $L \gtrsim 10^{48}$ erg s^{-1}; (3) they are observed in an extremely broad range of redshift $0 \lesssim z \lesssim 7$, and (4) they are stable compared to transients that are employed as distance indicators in cosmology, such as type Ia supernovæ (Section 2, Ref. [8] for a review). On the other hand, (1) quasars are anisotropic sources even if the degree of anisotropy is expected to be associated with the viewing angle of the accretion disk in radio-quiet quasars [9], and not large compared to radio-loud quasars whose optical continuum is in part beamed (see, for example [10]); (2) quasars have an open-ended luminosity function (i.e., without a clearly defined minimum, as the quasar highest spatial density occurs at the lowest luminosity); in other words, they are the "opposite" of a cosmological standard candle. In addition, (3) the long-term variability of radio-quiet quasars is poorly understood (see e.g., [11,12] and references therein) (4) and the internal structure of the active nucleus ($\lesssim$1000 r_g) is still a matter of debate (see, e.g., a summary of open issues [13] in [14]. Correlations with luminosity have been proved to be rather weak (see [15], for a synopsis up to mid-1999). The selection effect may even cancel out the "Baldwin effect" [16], a significant but weak anti-correlation between rest-frame equivalent width and continuum luminosity of CIVλ1549 that has been the most widely discussed luminosity correlation in the past several decades.

2. Definition of a Class of Type-1 Quasars with Properties of Eddington Standard Candles

Nonetheless, new developments in the past decades have paved the road to the possibility of exploiting quasars as cosmological distance indicators in a novel way that would make them literal "Eddington standard candles" (ESC) ([17–20]; see also [21] for a comprehensive review of secondary distance indicators including several techniques based on quasars). This possibility is based in the development of the concept of a quasar main sequence (MS), intended to provide a sort of H-R diagram for quasars [22]. The quasar MS can be traced in the plane defined by the prominence of optical FeII emission, $R_{\rm FeII}$ = I(FeIIλ 4570)/I(Hβ) (see [15,23–26]). Figure 1 provides a sketch of the MS in the optical plane FWHM(Hβ) vs. $R_{\rm FeII}$. It is possible to isolate spectral types in the optical plane of the MS as a function of $R_{\rm FeII}$ and FWHM Hβ and, at a coarser level, two populations: Population A (FWHM Hβ $<$ 4000 km/s) and Population B of broader sources. Pop. A is rather heterogeneous, and encompasses a range of $R_{\rm FeII}$ from almost 0 to the highest values observed ($R_{\rm FeII} \gtrsim 2$ are very rare, $\lesssim$1% in optically-selected samples, [25]). Along the quasar main sequence, the extreme Population A (xA) sources satisfying the condition $R_{\rm FeII} > 1$ (about 10% of all quasars in optically-selected sample, green area in Figure 1) show remarkably low optical variability, so low that it is even difficult to estimate the BLR radius via reverberation mapping [27]. This is at variance with Pop. B sources that show more pronounced variability [28,29], the most extreme cases being observed among blazars which are low-accretors, at the opposite end in the quasar MS. Of the many multi-frequency trends along the main sequence (from the sources whose spectra show the broadest LILs (extreme Pop.

B), and the weakest FeII emission, to sources with the narrowest LIL profiles and strongest FeII emission [extreme Pop. A]), we recall a systematic decrease of the CIV equivalent width, an increase in metallicity, and amplitude of HIL blueshifts (a more exhaustive list is provided by Table 1 of [30]). The Eddington ratio is believed to increase along with $R_{\rm FeII}$ [23,26,31,32]. The FWHM Hβ is strongly affected by the viewing angle (i.e., the angle between the line of sight and the accretion disk axis), so that at least the most narrow-line Seyfert 1s (NLSy1s) can be interpreted as Pop. A sources seen with the accretion disk oriented face-on or almost so [33]. At low-z ($\lesssim$0.7), Pop. A implies low black hole mass $M_{\rm BH}$, and high Eddington ratio; on the converse, Pop. B is associated with high $M_{\rm BH}$ and low $L/L_{\rm Edd}$. This trend follows from the "downsizing" of nuclear activity at low-z that helps give an elbow shape to the MS [34]: at low-z, very massive quasars ($M_{\rm BH} \gtrsim 10^9$ M$_\odot$) do not radiate close to their Eddington limit but are, conversely, low-radiators ($L/L_{\rm Edd} \lesssim 0.1$).

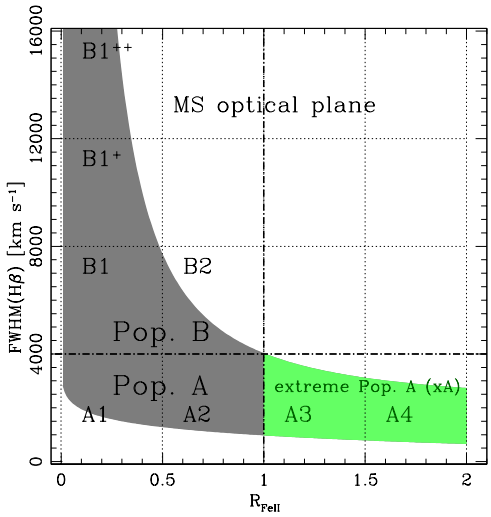

Figure 1. The plane FWHM(Hβ) vs. $R_{\rm FeII}$. The MS is sketched as the grey strip, with the section occupied by xA sources colored pale green. The thick dot-dashed line separates Pop. A and B at 4000 km s^{-1}, while the vertical one at $R_{\rm FeII}$ = 1 traces the $R_{\rm FeII}$ lower value for xA identification. The spectral types with significant occupation at low-z are labeled.

The inter-comparison between CIVλ1549 and Hβ supports low-ionization lines virial broadening (in a system of dense clouds or in the accretion disk) + high-ionization lines (HILs) radial or vertical outflows, at least in Pop. A sources [35,36]. There is now a wide consensus on an accretion disk + wind system model [37], and therefore on the existence of a "virialized" low-ionization subregion + higher ionization, with the subregion outflowing up to the highest quasar luminosities [36,38,39].

The most extreme examples at high accretion rate are a population of sources with distinguishing properties. They have been called extreme Pop. A or extreme quasars (xA), and are also known as super-Eddington accreting massive black holes (SEAMBHs) [9,18,40,41]. Figure 2 shows a composite rest-frame UV spectrum of high-luminosity xA quasars. Observationally, xA quasars satisfy $R_{\rm FeII} \geq 1$ and still show LIL Hβ profiles basically consistent with emission from a virialized system. xA quasars may well represent an early stage in the evolution of quasars and galaxies. In the hierarchical growth scenario for the evolution of galaxies, merging and strong interaction lead to accumulation of gas in the galaxy central regions, inducing enhanced star formation. Strong winds from massive stars and eventual Supernova explosions may ultimately provide enriched accretion fuel for the massive black hole at the galaxy [42–44]. The active nucleus radiation force and the mechanical thrust of the accretion disk wind can then sweep the dust surrounding the black hole, at least within a cone coaxial with the accretion disk axis (see Figure 7 of [45]). The fraction of mass that is accreted by the black hole and the fraction that is instead ejected in the wind are highly uncertain; the outflow kinetic power can become comparable to the radiative output [46,47], especially in sources accreting at very high

rate [48]; interestingly, this seems to be true also for stellar-mass black holes [49]. Feedback effects on the host galaxies are maximized by the high kinetic power of the wind, presumably made of gas much enriched in metals [50].

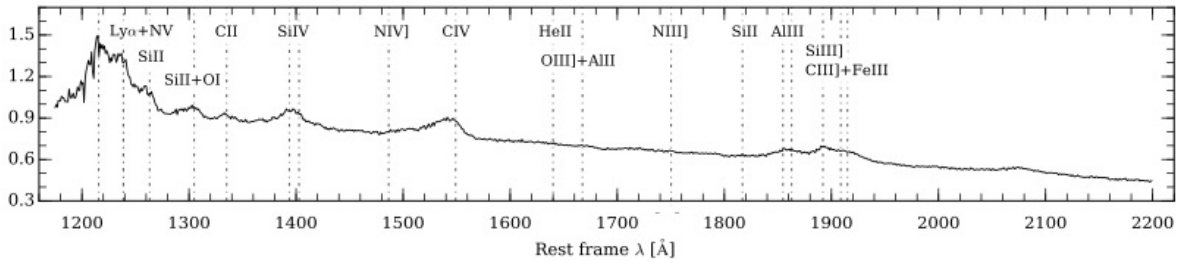

Figure 2. Composite UV spectrum of high-z xA sources. The abscissa is rest-frame wavelength, and the ordinate is normalized flux.

3. Diagnostics of Mildly-Ionized Gases

Diagnostics from the rest-frame UV spectrum takes advantage of the observations of strong resonance lines that are collisionally excited [51,52]. The point is that the rest-frame UV spectrum offers rich diagnostics that constrains at least gas density $n_{\rm H}$, ionization parameter U, and chemical abundance Z. For instance, Si IIλ 1814/Si III]λ 1892 is sensitive to ionization CIVλ1549/Lyα, CIVλ1549/(Si IV + OIV])λ1400, CIVλ1549/HeIIλ1640, NVλ1240/HeIIλ1640 are sensitive to metallicity; and Al IIIλ1860/Si III]λ1892, Si III]λ1892/CIII]λ1909 are sensitive to density, since inter-combination lines have a well defined critical density [51].

The photoionization code *Cloudy* models the ionization, chemical, and thermal state of gas exposed to a radiation field, and predicts its emission spectra and physical parameters [53,54]. In *Cloudy*, collisional excitation and radiative processes typical of mildly ionized gases are included. *Cloudy* simulation requires inputs in terms of $n_{\rm H}$, U, Z, quasar spectral energy distribution (SED), and column density $N_{\rm c}$. The ionization parameter

$$U = \frac{\int_{\nu_0}^{\infty} \frac{L_\nu}{h\nu}}{4\pi r_{\rm BLR}^2 c n_{\rm H}} = \frac{Q(H)}{4\pi r_{\rm BLR}^2 c n_{\rm H}}, \quad (1)$$

where $Q(H)$ is the number of ionizing photons, provides the ratio between photon and hydrogen number density. More importantly, the inversion of equation provides a measure of the emitting region radius $r_{\rm BLR}$ once the ionizing photon flux i.e., the product Un_H is known. As we will see, the photon flux can be estimated with good precision from diagnostic line intensity ratios.

Maps built on an array of 551 Cloudy 08.00–13.00 photoionization models for a given metallicity Z and $N_{\rm c}$, constant n and U evaluated at steps of 0.25 dex covering the ranges $7 \leq \log n_{\rm H} \leq 14$ [cm^{-3}], $-4.5 \leq \log U \leq 0$. Given the measured intensity ratios for xA quasars, *Cloudy* simulations show convergence toward a well-defined value of log ($n_{\rm H}U$) [40,51]. UV diagnostic ratios in the plane ionization parameter versus density indicate extremely high $n_{\rm H}$ $10^{12.5–13}$ cm^{-3}, extremely low $\log U \sim -2.5$–3 (Figure 3). Note the orthogonal information provided by the AlIIIλ1860/SiIII]λ1892 that mainly depends on density. The left and right panels differ because of chemical abundances: the case with five times solar metallicity plus overabundance of Si and Al produces better agreement, displacing the solution toward lower density and higher ionization. Nonetheless, the product $Un_{\rm H}$ remains fairly constant. Diagnostic ratios sensible to chemical composition suggest high metallicity. The metallicities in the quasar BLR gas are a function of the spectral type (ST) along the MS: relatively low (solar or slightly sub-solar in extreme Pop. B sources (as estimated recently for NGC 1275 [55]), and relatively high for typical Pop. A quasars with moderate FeII emission ($Z \sim$ 5–10$Z_\odot$, [56,57]). If the diagnostic ratios are interpreted in terms of scaled $Z_\odot$, they may reach $Z \gtrsim 20Z_\odot$, even $Z \sim 100Z_\odot$ for xA quasars [40]. Z values as high as $Z \sim 100Z_\odot$ are likely to be unphysical, and suggest relative

abundances of elements deviating from solar values, as assumed in the previous example, or significant turbulence. The analysis of the gas chemical composition in the BLR of xA source has just begun. However, high or non-solar Z are in line with the idea of xA sources being high accretors surrounded by huge amount of gas and a circum-nuclear star forming system, possibly with a top-heavy initial mass function [51]. The high $n_{\rm H}$ is consistent with the low CIII]λ1909 emission that becomes undetectable in some cases. While in Pop. A and B we find evidence of ionization stratification within the low-ionization part of the BLR ([58–60] and references therein), xA sources show intensity ratios that are consistent with a very dense "remnant" of the BLR, perhaps after lower density gas has been ablated away by radiation forces.

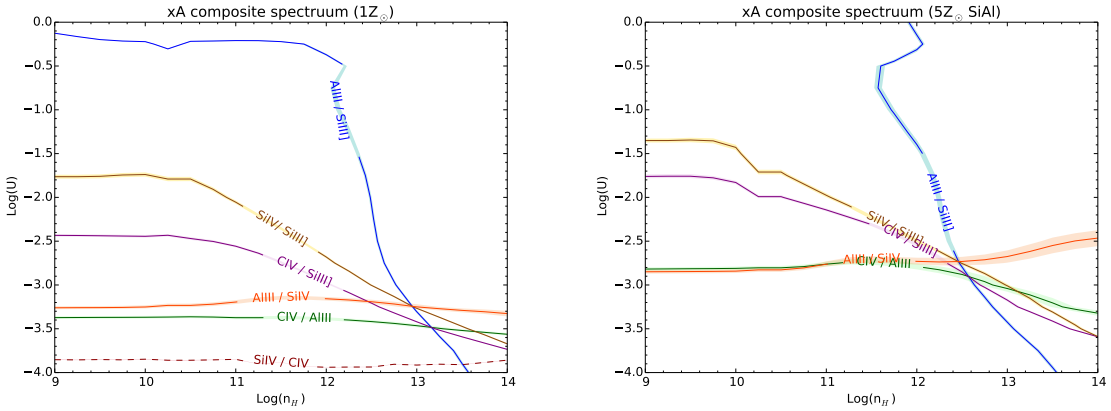

Figure 3. Intensity ratios in the plane ionization parameter vs. density, for the intensity ratios measured on the composite xA quasar spectrum shown in Figure 2 of [40]. left panel: solar chemical composition; right: 5$\times$ solar chemical composition with selective enrichment in Al and Si, following [51]. In this latter case, the SiIVλ1402/CIVλ1549 is degenerate.

4. xA Quasars as Eddington Standard Candles

There are several key elements that make it possible to exploit xA quasars as Eddington standard candles.

The first is the similarity of their spectra and hence of the physical condition in the mildly-ionized gas that is emitting the LILs. Line intensity ratios are similar (they scatter around a constant average with small dispersion). Since the line emitting gas is photoionized, intensity line ratios depend strongly on the ionizing continuum SED. Thus, the ionizing SED is also constrained within a small scatter. We remark that this is not true for the general population of quasars that show differences in line equivalent width and intensity ratios larger than an order of magnitude along the MS.

The mass reservoir in all xA sources is sufficient to ensure a very high accretion rate (possibly super-Eddington) that yields a radiative output close to the Eddington limit. The similarity of the SED and the presence of high rates of circumnuclear and galactic star formation as revealed by Spitzer [61] have led to the conjecture that xA sources may be in a particular stage of a quasar development, as mentioned above.

The second key element is the existence of a virialized low-ionization sub-region (possibly the accretion disk itself). This region coexists with outflowing gas even at extreme $L \gtrsim 10^{48}$ erg s^{-1} and highest Eddington ratios but is kinematically distinguishable on the basis of inter-line shifts between LILs and HILs—for example, Hβ and CIVλ1549.

In addition, xA quasars show extreme $L/L_{\rm Edd}$ along the MS with small dispersion. If the Eddington ratio is known, and constant, then $\lambda = L/L_{\rm Edd} \propto L/M_{\rm BH}$. Accretion disk theory teaches low radiative efficiency at a high accretion rate, and that λ saturates toward a limiting value ([62–64] and references therein). Therefore, empirical evidence (the xA class of sources, easily identified by their self-similar properties, scatters around a well-defined, extremal λ) and theoretical support

(the saturation of the radiative output per unit $M_{\rm BH}$) justified the consideration of xA sources potential ESCs.

Virial Luminosity

The use of xA sources as Eddington standard candles requires several steps which should considered carefully.

1. The first step is the actual estimate of the accretion luminosity via a virial broadening estimator (VBE). The luminosity can be written as

$$L \propto \text{ל} M_{\rm BH} \propto \text{ל} r_{\rm BLR} (\delta v)^2, \tag{2}$$

   assuming virial motions of the low-ionionization part of the broad-line region (BLR). The δv stands for a suitable VBE, usually the width of a convenient LIL (in practice, the FWHM of Hβ or even Paα, [65]).
2. The $r_{\rm BLR}$ can be estimated from the inversion of Equation (1) [51,52], again taking advantage of the fact that the ionizing photon flux shows a small scatter around a well defined value. In addition, another key assumption is that

$$r_{\rm BLR} \propto \left(\frac{L}{n_{\rm H} U} \right)^{\frac{1}{2}}. \tag{3}$$

   Equation (3) implies that $r_{\rm BLR}$ scales with the square root of the luminosity. This is needed to preserve the U parameter. If U were going to change, then the spectrum would also change as a function of luminosity. This is not evident comparing spectra over a wide luminosity range (4.5 dex), although some second order effects are possible.[1]
3. We can therefore write the virial luminosity as

$$L \propto \text{ל} \left(\frac{L}{n_{\rm H} U} \right)^{\frac{1}{2}} (\delta v)^2. \tag{4}$$

   Making explicit the dependence of the number of ionizing photons on the SED, the virial luminosity becomes:

$$L \approx 7.8 \cdot 10^{44} \frac{\text{ל}_1^2 \kappa_{0.5} f_2^2}{\tilde{\nu}_{2.42 \cdot 10^{16}}} \frac{1}{(n_{\rm H} U)_{9.6}} (\delta v_{1000})^4, \tag{5}$$

   where κ is the fraction of ionizing luminosity scaled to 0.5, $\tilde{\nu}$ the average frequency of ionizing photons scaled to $2.42 \cdot 10^{16}$ Hz, and $(n_{\rm H} U)$ to $10^{9.6}$.

Equation (5) is analogous to the Tully–Fisher [66] and the early formulation of the Faber–Jackson [67] laws for galaxies. Equation (5) is applicable to xA quasars with Eddington ratio $\text{ל} \sim 1$ and dispersion $\delta \text{ל} \ll 1$ but, in principle, could be used for every sample of quasars whose ל is in a very restricted range.

5. Selection of Eddington Standard Candles

Selection criteria are based on emission line intensity ratios which are extreme along the quasar MS [20]:

[1] The maximum temperature of the accretion disk is $\propto M_{\rm BH}^{-\frac{1}{2}}$; the SED is expected to become softer at high $M_{\rm BH}$, but this effect has not been detected yet at a high confidence level.

1. $R_{\rm FeII} > 1.0$,
2. UV AlIIIλ1860/SiIII]λ1892 > 0.5,
3. SiIII]λ1892/CIII]λ1909 > 1.

The first criterion can be easily applied to optical spectra of a large survey such as the SDSS for sources at $z \lesssim 1$. The second and third criterion can be applied to sources at $1 \lesssim z \lesssim 4.5$ for which the 1900 blend lines are shifted into the optical and near IR domains. UV and optical selection criterions are believed to be equivalent. Due to a small sample size at low z for which rest-frame optical and UV spectra are available, further testing is needed.

6. Tentative Applications to Cosmology and the Future Perspectives

Preliminary results were collected from three quasar samples (62 sources in total), unevenly covering the redshift range $0.4 \lesssim z \lesssim 2.6$. For redshift $z \gtrsim 2$, the UV AlIIIλ1860 FWHM was used as a VBE for the rest-frame UV range, save a few cases for which Hβ was available. This explorative application to cosmology yielded results consistent with concordance cosmology, and allowed the exclusion of some extreme cosmologies [20]. A more recent application involved the [20] sample, along with the Hβ sample of [9] and preliminary measurements from [40]. The resulting Hubble diagram is shown in Figure 4. The plots in Figure 4 involve $\approx$ 220 sources and indicate a scatter $\delta\mu \approx 1.2$ mag. The slope of the residuals ($b \approx -0.002 \pm 0.104$) is not significantly different from 0, indicating good statistical agreement between luminosities derived from concordance cosmological parameters and from the virial equation. The Hubble diagram of Figure 4 confirms the conceptual validity of the virial luminosity relation, Equation (5).

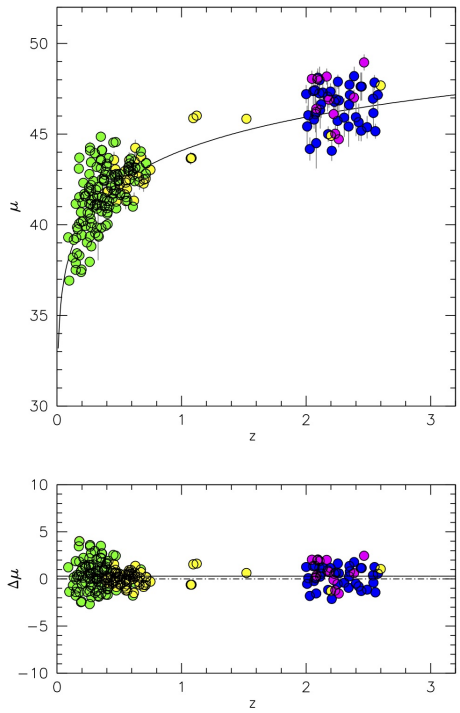

Figure 4. Hubble diagram distance modulus μ vs. z obtained from the analysis of the [20] data (yellow: Hβ, navy blue: AlIIIλ1860 and SiIII]λ1892) supplemented by new Hβ measurements from the SDSS obtained in this work (green) and from Gran Telescopio Canarias (GTC) observations of Martinez-Aldama et al. [68] (magenta). The lower panel shows the distance modulus residuals with respect to concordance cosmology. The filled line in the upper panel is the $\mu(z)$ expected from Λ cold dark matter (CDM) cosmology. The filled line in the lower panel represents a least-square fit to the residuals as a function of z. The figure is an updated version of Figure 1 of Marziani et al. [69].

Mock samples of several hundreds of objects, even with significant dispersion in luminosity with rms(log L) = 0.2–0.3, indicate that quasars covering the redshift range between 0 and 3 (i.e., a range of cosmic epochs from now to 2 Gyr since the Big Bang) could yield significant constraints on the cosmological parameters. A synthetic sample of 200 sources uniformly distributed in the redshift range 0–3 with a scatter of 0.2 dex yields $\Omega_{\rm M} \approx 0.28 \pm 0.02$ at 1σ confidence level, assuming $H_0 = 70$ km s^{-1} Mpc^{-1}, and flatness ($\Omega_M + \Omega_\Lambda$=1). If $\Omega_M + \Omega_\Lambda$ is unconstrained, $\Omega_{\rm M} \approx 0.30^{+0.12}_{-0.09}$ at 1σ confidence level [20]. The comparison between the constraints set by supernova surveys and by a mock sample of 400 quasars with rms = 0.3 dex in log L shows the potential ability of the quasar sample to better constrain Ω_M [70]. The scheme of Figure 5 illustrates the difference in sensitivity to cosmological parameters over the redshift range 0–4: supernovæ are sensitive to Ω_Λ since the effect of Ω_Λ, in a concordance cosmology scenario, became appreciable only at relatively recent cosmic epochs. High redshift quasars provide information on a redshift range where the expansion of the Universe was still being decelerated by the effect of Ω_M, a range that is not yet covered by any standard ruler or candle.

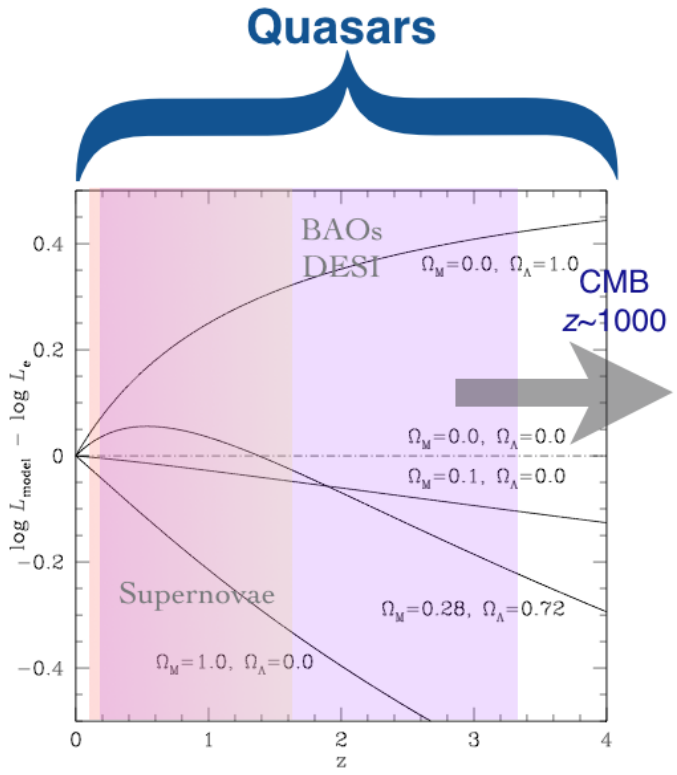

Figure 5. Luminosity difference with respect to an empty Universe for several cosmological models, identified by their values of Ω_M and Ω_Λ. The domain of supernovæ and of the baryonic acoustic oscillations (within the expectation of the future Dark Energy Spectroscopic Instrument (DESI) survey, [71]) are shown.

Error Budget

The large scatter in the luminosity estimates is apparently daunting in the epoch of precision cosmology. Statistical errors could be reduced to rms $\approx$ 0.2 dex in L by increasing numbers, collecting large samples ($\sim$500 quasars), but they still would remain high.

The xA quasar SED cannot vary much since spectra are almost identical in terms of line ratios (a second order effect [72] not yet detected as significant in the data considered by [20,40] may become significant with larger samples). The scaling $r_{\rm BLR} \propto L^{0.5}$ should hold strictly: a small deviation would imply a systematic change in the ionization parameter and hence of ST with luminosity.

A simplified error budget for statistical errors [20] indicates that virial luminosity estimates are mostly affected by VBE uncertainties which enter with the fourth power in Equation (5). In addition to measurement uncertainties, orientation effects are expected to be determinant in the FWHM uncertainties, as they can contribute 0.3 dex of scatter in luminosity if Hβ or any other line used as a VBE is emitted in a highly-flattened configuration.[2] Modeling the effect of orientation by computing the difference between L from concordance cosmology and virial luminosity indeed reduces the sample standard deviation in the Hubble diagram by a factor $\approx$5 to $\approx$0.2 mag, and accounts for most of the rms $\approx$ 0.4 dex in the virial luminosity estimates of the sample shown in Figure 4 [9]. The rms $\approx$ 0.2 mag value is comparable to the uncertainty in supernova magnitude measurements. Work is in progress in order to make viewing angle estimates of xA quasars usable for cosmology.

7. Conclusions

This paper provided an overview of the physical conditions in the broad line emitting region of extreme spectral types of type-1 quasars (the extreme Pop. A). There is strong evidence that xA sources are radiating close to their Eddington limit (i.e., with Eddington ratio scattering around a well-defined value), at high accretion rates. Their physical properties appear to be very stable across a very wide range of luminosity, 4–5 dex. The assumption of a constant $\daleth$ makes it possible to write a relation between luminosity and virial broadening, analogous to the one expressed by the Tully–Fisher and the early formulation of Faber–Jackson laws.

The scatter in the Hubble diagram obtained from virial luminosity estimates is still very high, about 1 mag (although comparable to the scatter from a method based on the nonlinear relation between the X-ray and the UV emission of quasars [75]). Very large samples are needed for reduction of scatter (and statistical error). In addition, the inter-calibration of rest-frame visual and UV properties and their dependence on L (expect systematic errors!) needs to be extended by dedicated observations of xA sources covering the rest frame UV and visual range. Simulations of statistical and systematic effects which influence the estimates of the cosmic parameters are also needed.

In principle, Eddington standard candles can cover a range of distances where the metric of the Universe has not been "charted" as yet to retrieve an independent estimate of $\Omega_{\rm M}$. If samples with uniform coverage over a wide range of redshift would become available, xA sources could also address the physics of accelerated expansion (i.e., provide measurements of the dark energy equation of state).

Author Contributions: E.B., N.B., A.d.O. and D.D. contributed with funding acquisition and resources. P.M., E.B., N.B., A.d.O., M.L.M.-A., C.A.N., M.D., G.M.S. significantly contributed to the papers on which this review is based. P.M. wrote the review paper.

Funding: P.M. wishes to thank the Scientific Organizing Committee of the Symposium on the Physics of Ionized Gases (SPIG 2018) meeting for inviting the topical lecture on which this paper is based, and acknowledges the Programa de Estancias de Investigación (PREI) No. DGAP/DFA/2192/2018 of Universidad Nacional Autónoma de México (UNAM), where this paper was written. The relevant research is part of the project 176001 "Astrophysical spectroscopy of extragalactic objects" and 176003 "Gravitation and the large scale structure of the Universe" supported by the Ministry of Education, Science and Technological Development of the Republic of Serbia. M.L.M.-A. acknowledges a CONACyT postdoctoral fellowship. A.d.O. and M.L.M.-A. acknowledge financial support from the Spanish Ministry for Economy and Competitiveness through Grant Nos. AYA2013-42227-P and AYA2016-76682-C3-1-P. M.L.M.-A, P.M. and M.D. acknowledge funding from the INAF PRIN-SKA 2017 program 1.05.01.88.04. D.D. and A.N. acknowledge support from CONACyT through Grant No. CB221398. D.D. and C.A.N. are also thankful for the support from Grant No. IN108716 53 PAPIIT, UNAM.

Conflicts of Interest: The authors declare no conflict of interest.

[2] The $M_{\rm BH}$ is not computed explicitly for the estimate of L following Equation (5). However, the VBE uncertainty associated with orientation is the main source of uncertainty on $M_{\rm BH}$ for the xA sample. This is most likely the case also for the general quasar population [73,74].

Abbreviations

The following abbreviations are used in this manuscript:

AGN	Active Galactic Nucleus
BLR	Broad Line Region
DESI	Dark Energy Spectroscopic Instrument
ESC	Eddington Standard Candles
FWHM	Full Width Half-Maximum
HIL	High-Ionization Line
LIL	Low-Ionization Line
MDPI	Multidisciplinary Digital Publishing Institute
MS	Main Sequence
NLSy1	Narrow-Line Seyfert 1
SDSS	Sloan Digital Sly Survey
VBE	Virial Broadening Estimator

References

1. Vanden Berk, D.E.; Richards, G.T.; Bauer, A.; Strauss, M.A.; Schneider, D.P.; Heckman, T.M.; York, D.G.; Hall, P.B.; Fan, X.; Knapp, G.R.; et al. Composite Quasar Spectra from the Sloan Digital Sky Survey. *Astron. J.* **2001**, *122*, 549–564. [CrossRef]
2. Marziani, P.; Dultzin-Hacyan, D.; Sulentic, J.W. Accretion onto Supermassive Black Holes in Quasars: Learning from Optical/UV Observations. In *New Developments in Black Hole Research*; Kreitler, P.V., Ed.; Nova Press: New York, NY, USA, 2006; p. 123.
3. Netzer, H. AGN emission lines. In *Active Galactic Nuclei*; Blandford, R.D., Netzer, H., Woltjer, L., Courvoisier, T.J.-L., Mayor, M., Eds.; Springer: Berlin/Heidelberg, Germany, 1990; pp. 57–160.
4. Marinello, A.O.M.; Rodriguez-Ardila, A.; Garcia-Rissmann, A.; Sigut, T.A.A.; Pradhan, A.K. The FeII emission in active galactic nuclei: Excitation mechanisms and location of the emitting region. *arXiv* **2016**, arXiv:1602.05159.
5. Antonucci, R. Unified models for active galactic nuclei and quasars. *Annu. R. Astron. Astrophys.* **1993**, *31*, 473–521. [CrossRef]
6. D'Onofrio, M.; Burigana, C. *Questions of Modern Cosmology: Galileo's Legacy*; Springer: Berlin/Heidelberg, Germany, 2009. [CrossRef]
7. Pâris, I.; Petitjean, P.; Aubourg, É.; Myers, A.D.; Streblyanska, A.; Lyke, B.W.; Anderson, S.F.; Armengaud, É.; Bautista, J.; Blanton, M.R.; et al. The Sloan Digital Sky Survey Quasar Catalog: Fourteenth data release. *Astron. Astrophys.* **2018**, *613*, A51. [CrossRef]
8. Marziani, P.; Dultzin, D.; Sulentic, J.W.; Del Olmo, A.; Negrete, C.A.; Martinez-Aldama, M.L.; D'Onofrio, M.; Bon, E.; Bon, N.; Stirpe, G.M. A main sequence for quasars. *Front. Astron. Space Sci.* **2018**, *5*, 6. [CrossRef]
9. Negrete, C.A.; Dultzin, D.; Marziani, P.; Esparza, D.; Sulentic, J.W.; del Olmo, A.; Martínez-Aldama, M.L.; García López, A.; D'Onofrio, M.; Bon, N.; et al. Highly accreting quasars: The SDSS low-redshift catalog. *Astron. Astrophys.* **2018**, *620*, A118. [CrossRef]
10. Liu, Y.; Jiang, D.R.; Gu, M.F. The Jet Power, Radio Loudness, and Black Hole Mass in Radio-loud Active Galactic Nuclei. *Astrophys. J.* **2006**, *637*, 669–681. [CrossRef]
11. Bon, E.; Zucker, S.; Netzer, H.; Marziani, P.; Bon, N.; Jovanović, P.; Shapovalova, A.I.; Komossa, S.; Gaskell, C.M.; Popović, L.Č.; et al. Evidence for Periodicity in 43 year-long Monitoring of NGC 5548. *Astrophys. J. Suppl. Ser.* **2016**, *225*, 29. [CrossRef]
12. Bon, E.; Marziani, P.; Bon, N. Periodic optical variability of AGN. *IAU Symp.* **2017**, *324*, 176–179. [CrossRef]
13. Netzer, H. Meeting Summary: A 2017 View of Active Galactic Nuclei. *Front. Astron. Space Sci.* **2018**, *5*, 10. [CrossRef]
14. Marziani, P.; D'Onofrio, M.; del Olmo, A.; Dultzin, D. (Eds.) *Quasars at All Cosmic Epochs*; Frontiers Media: Lausanne, Switzerland, 2018. [CrossRef]
15. Sulentic, J.W.; Marziani, P.; Dultzin-Hacyan, D. Phenomenology of Broad Emission Lines in Active Galactic Nuclei. *Annu. Rev. Astron. Astrophys.* **2000**, *38*, 521–571. [CrossRef]

16. Baldwin, J.A.; Burke, W.L.; Gaskell, C.M.; Wampler, E.J. Relative quasar luminosities determined from emission line strengths. *Nature* **1978**, *273*, 431–435. [CrossRef]
17. Teerikorpi, P. On Öpik's distance evaluation method in a cosmological context. *Astron. Astrophys.* **2011**, *531*, A10. [CrossRef]
18. Wang, J.M.; Du, P.; Valls-Gabaud, D.; Hu, C.; Netzer, H. Super-Eddington Accreting Massive Black Holes as Long-Lived Cosmological Standards. *Phys. Rev. Lett.* **2013**, *110*, 081301. [CrossRef] [PubMed]
19. Wang, J.M.; Du, P.; Li, Y.R.; Ho, L.C.; Hu, C.; Bai, J.M. A New Approach to Constrain Black Hole Spins in Active Galaxies Using Optical Reverberation Mapping. *Astrophys. J. Lett.* **2014**, *792*, L13. [CrossRef]
20. Marziani, P.; Sulentic, J.W. Highly accreting quasars: Sample definition and possible cosmological implications. *Mon. Not. R. Astron. Soc.* **2014**, *442*, 1211–1229. [CrossRef]
21. Czerny, B.; Beaton, R.; Bejger, M.; Cackett, E.; Dall'Ora, M.; Holanda, R.F.L.; Jensen, J.B.; Jha, S.W.; Lusso, E.; Minezaki, T.; et al. Astronomical Distance Determination in the Space Age. Secondary Distance Indicators. *Space Sci. Rev.* **2018**, *214*, 32. [CrossRef]
22. Sulentic, J.W.; Zamfir, S.; Marziani, P.; Dultzin, D. Our Search for an H-R Diagram of Quasars. *Revista Mexicana de Astronomia y Astrofisica Conference Series* **2008**, *32*, 51–58.
23. Boroson, T.A.; Green, R.F. The emission-line properties of low-redshift quasi-stellar objects. *Astrophys. J. Suppl. Ser.* **1992**, *80*, 109–135. [CrossRef]
24. Sulentic, J.W.; Marziani, P.; Zamanov, R.; Bachev, R.; Calvani, M.; Dultzin-Hacyan, D. Average Quasar Spectra in the Context of Eigenvector 1. *Astrophys. J. Lett.* **2002**, *566*, L71–L75. [CrossRef]
25. Zamfir, S.; Sulentic, J.W.; Marziani, P.; Dultzin, D. Detailed characterization of Hβ emission line profile in low-z SDSS quasars. *Mon. Not. R. Astron. Soc.* **2010**, *403*, 1759. [CrossRef]
26. Shen, Y.; Ho, L.C. The diversity of quasars unified by accretion and orientation. *Nature* **2014**, *513*, 210–213. [CrossRef] [PubMed]
27. Du, P.; Zhang, Z.X.; Wang, K.; Huang, Y.K.; Zhang, Y.; Lu, K.X.; Hu, C.; Li, Y.R.; Bai, J.M.; Bian, W.H.; et al. Supermassive Black Holes with High Accretion Rates in Active Galactic Nuclei. IX. 10 New Observations of Reverberation Mapping and Shortened Hβ Lags. *Astrophys. J.* **2018**, *856*, 6. [CrossRef]
28. Dultzin-Hacyan, D.; Schuster, W.J.; Parrao, L.; Pena, J.H.; Peniche, R.; Benitez, E.; Costero, R. Optical variability of the Seyfert nucleus NGC 7469 in timescales from days to minutes. *Astron. J.* **1992**, *103*, 1769–1787. [CrossRef]
29. Giveon, U.; Maoz, D.; Kaspi, S.; Netzer, H.; Smith, P.S. Long-term optical variability properties of the Palomar-Green quasars. *Mon. Not. R. Astron. Soc.* **1999**, *306*, 637–654. [CrossRef]
30. Sulentic, J.; Marziani, P.; Zamfir, S. The Case for Two Quasar Populations. *Balt. Astron.* **2011**, *20*, 427–434. [CrossRef]
31. Kuraszkiewicz, J.K.; Green, P.J.; Crenshaw, D.M.; Dunn, J.; Forster, K.; Vestergaard, M.; Aldcroft, T.L. Emission Line Properties of Active Galactic Nuclei from a Post-COSTAR Hubble Space Telescope Faint Object Spectrograph Spectral Atlas. *Astrophys. J. Suppl. Ser.* **2004**, *150*, 165–180. [CrossRef]
32. Sun, J.; Shen, Y. Dissecting the Quasar Main Sequence: Insight from Host Galaxy Properties. *Astrophys. J. Lett.* **2015**, *804*, L15. [CrossRef]
33. Dultzin, D.; Martinez, M.L.; Marziani, P.; Sulentic, J.W.; Negrete, A. Narrow-Line Seyfert 1s: A luminosity dependent definition. In Proceedings of the Conference "Narrow-Line Seyfert 1 Galaxies and Their Place in the Universe", Milano, Italy, 4–6 April 2011.
34. Fraix-Burnet, D.; Marziani, P.; D'Onofrio, M.; Dultzin, D. The Phylogeny of Quasars and the Ontogeny of Their Central Black Holes. *Front. Astron. Space Sci.* **2017**, *4*, 1. [CrossRef]
35. Leighly, K.M. Hubble Space Telescope STIS Ultraviolet Spectral Evidence of Outflow in Extreme Narrow-Line Seyfert 1 Galaxies. II. Modeling and Interpretation. *Astrophys. J.* **2004**, *611*, 125–152. [CrossRef]
36. Sulentic, J.W.; del Olmo, A.; Marziani, P.; Martínez-Carballo, M.A.; D'Onofrio, M.; Dultzin, D.; Perea, J.; Martínez-Aldama, M.L.; Negrete, C.A.; Stirpe, G.M.; et al. What does Civλ1549 tell us about the physical driver of the Eigenvector Quasar Sequence? *arXiv* **2017**, arXiv:1708.03187.
37. Elvis, M. A Structure for Quasars. *Astrophys. J.* **2000**, *545*, 63–76. [CrossRef]
38. Bisogni, S.; di Serego Alighieri, S.; Goldoni, P.; Ho, L.C.; Marconi, A.; Ponti, G.; Risaliti, G. Simultaneous detection and analysis of optical and ultraviolet broad emission lines in quasars at z 2.2. *arXiv* **2017**, arXiv:1702.08046.

39. Vietri, G.; Piconcelli, E.; Bischetti, M.; Duras, F.; Martocchia, S.; Bongiorno, A.; Marconi, A.; Zappacosta, L.; Bisogni, S.; Bruni, G.; et al. The WISSH Quasars Project IV. BLR versus kpc-scale winds. *arXiv* **2018**, arXiv:1802.03423.
40. Martínez-Aldama, M.L.; Del Olmo, A.; Marziani, P.; Sulentic, J.W.; Negrete, C.A.; Dultzin, D.; D'Onofrio, M.; Perea, J. Extreme quasars at high redshift. *Astron. Astroph.* **2018**, *618*, A179. [CrossRef]
41. Du, P.; Lu, K.X.; Hu, C.; Qiu, J.; Li, Y.R.; Huang, Y.K.; Wang, F.; Bai, J.M.; Bian, W.H.; Yuan, Y.F.; et al. Supermassive Black Holes with High Accretion Rates in Active Galactic Nuclei. VI. Velocity-resolved Reverberation Mapping of the Hβ Line. *Astrophys. J.* **2016**, *820*, 27. [CrossRef]
42. Heller, C.H.; Shlosman, I. Fueling nuclear activity in disk galaxies: Starbursts and monsters. *Astrophys. J.* **1994**, *424*, 84–105. [CrossRef]
43. Collin, S.; Zahn, J.P. Star formation and evolution in accretion disks around massive black holes. *Annu. Rev. Astron. Astrophys.* **1999**, *344*, 433–449.
44. Williams, R.J.R.; Baker, A.C.; Perry, J.J. Symbiotic starburst-black hole active galactic nuclei—I. Isothermal hydrodynamics of the mass-loaded interstellar medium. *Mon. Not. R. Astron. Soc.* **1999**, *310*, 913–962. [CrossRef]
45. D'Onofrio, M.; Marziani, P. A Multimessenger View of Galaxies and Quasars From Now to Mid-century. *Front. Astron. Space Sci.* **2018**, *5*, 31. [CrossRef]
46. King, A.; Pounds, K. Powerful Outflows and Feedback from Active Galactic Nuclei. *Annu. R. Astron. Astrophys.* **2015**, *53*, 115–154. [CrossRef]
47. Marziani, P.; Negrete, C.A.; Dultzin, D.; Martínez-Aldama, M.L.; Del Olmo, A.; D'Onofrio, M.; Stirpe, G.M. Quasar massive ionized outflows traced by CIV λ1549 and [OIII]$\lambda\lambda$4959,5007. *Front. Astron. Space Sci.* **2017**, *4*, 16. [CrossRef]
48. Nardini, E.; Reeves, J.N.; Gofford, J.; Harrison, F.A.; Risaliti, G.; Braito, V.; Costa, M.T.; Matzeu, G.A.; Walton, D.J.; Behar, E.; et al. Black hole feedback in the luminous quasar PDS 456. *Science* **2015**, *347*, 860–863. [CrossRef] [PubMed]
49. Tetarenko, B.E.; Lasota, J.P.; Heinke, C.O.; Dubus, G.; Sivakoff, G.R. Strong disk winds traced throughout outbursts in black-hole X-ray binaries. *Nature* **2018**, *554*, 69. [CrossRef] [PubMed]
50. Baskin, A.; Laor, A. Metal enrichment by radiation pressure in active galactic nucleus outflows - theory and observations. *Mon. Not. R. Astron. Soc.* **2012**, *426*, 1144–1158. [CrossRef]
51. Negrete, A.; Dultzin, D.; Marziani, P.; Sulentic, J. BLR Physical Conditions in Extreme Population A Quasars: A Method to Estimate Central Black Hole Mass at High Redshift. *Astrophys. J.* **2012**, *757*, 62. [CrossRef]
52. Negrete, C.A.; Dultzin, D.; Marziani, P.; Sulentic, J.W. Reverberation and Photoionization Estimates of the Broad-line Region Radius in Low-z Quasars. *Astrophys. J.* **2013**, *771*, 31. [CrossRef]
53. Ferland, G.J.; Porter, R.L.; van Hoof, P.A.M.; Williams, R.J.R.; Abel, N.P.; Lykins, M.L.; Shaw, G.; Henney, W.J.; Stancil, P.C. The 2013 Release of Cloudy. *Revista Mexicana de Astronomía y Astrofísica* **2013**, *49*, 137–163.
54. Ferland, G.J.; Chatzikos, M.; Guzmán, F.; Lykins, M.L.; van Hoof, P.A.M.; Williams, R.J.R.; Abel, N.P.; Badnell, N.R.; Keenan, F.P.; Porter, R.L.; et al. The 2017 Release Cloudy. *Revista Mexicana de Astronomía y Astrofísica* **2017**, *53*, 385–438.
55. Punsly, B.; Marziani, P.; Bennert, V.N.; Nagai, H.; Gurwell, M.A. Revealing the Broad Line Region of NGC 1275: The Relationship to Jet Power. *Astrophys. J.* **2018**, *869*, 143. [CrossRef]
56. Shin, J.; Woo, J.H.; Nagao, T.; Kim, S.C. The Chemical Properties of Low-redshift QSOs. *Astrophys. J.* **2013**, *763*, 58. [CrossRef]
57. Sulentic, J.W.; Marziani, P.; del Olmo, A.; Dultzin, D.; Perea, J.; Alenka Negrete, C. GTC spectra of z $\approx$ 2.3 quasars: Comparison with local luminosity analogs. *Astron. Astrophys.* **2014**, *570*, A96. [CrossRef]
58. Peterson, B.M.; Wandel, A. Evidence for Supermassive Black Holes in Active Galactic Nuclei from Emission-Line Reverberation. *Astrophys. J. Lett.* **2000**, *540*, L13–L16. [CrossRef]
59. Peterson, B.M.; Wandel, A. Keplerian Motion of Broad-Line Region Gas as Evidence for Supermassive Black Holes in Active Galactic Nuclei. *Astrophys. J. Lett.* **1999**, *521*, L95–L98. [CrossRef]
60. Gaskell, C.M. What broad emission lines tell us about how active galactic nuclei work. *New Astron. Rev.* **2009**, *53*, 140–148. [CrossRef]
61. Sani, E.; Lutz, D.; Risaliti, G.; Netzer, H.; Gallo, L.C.; Trakhtenbrot, B.; Sturm, E.; Boller, T. Enhanced star formation in narrow-line Seyfert 1 active galactic nuclei revealed by Spitzer. *Mon. Not. R. Astron. Soc.* **2010**, *403*, 1246–1260. [CrossRef]

62. Abramowicz, M.A.; Czerny, B.; Lasota, J.P.; Szuszkiewicz, E. Slim accretion disks. *Astrophys. J.* **1988**, *332*, 646–658. [CrossRef]
63. Mineshige, S.; Kawaguchi, T.; Takeuchi, M.; Hayashida, K. Slim-Disk Model for Soft X-Ray Excess and Variability of Narrow-Line Seyfert 1 Galaxies. *Publ. Astron. Soc. Jpn.* **2000**, *52*, 499–508. [CrossRef]
64. Abramowicz, M.A.; Straub, O. Accretion discs. *Scholarpedia* **2014**, *9*, 2408. [CrossRef]
65. La Franca, F.; Bianchi, S.; Ponti, G.; Branchini, E.; Matt, G. A New Cosmological Distance Measure Using Active Galactic Nucleus X-Ray Variability. *Astrophys. J. Lett.* **2014**, *787*, L12. [CrossRef]
66. Tully, R.B.; Fisher, J.R. A new method of determining distances to galaxies. *Astron. Astrophys.* **1977**, *54*, 661–673.
67. Faber, S.M.; Jackson, R.E. Velocity dispersions and mass-to-light ratios for elliptical galaxies. *Astrophys. J.* **1976**, *204*, 668–683. [CrossRef]
68. Martínez-Aldama, M.L.; Del Olmo, A.; Marziani, P.; Sulentic, J.W.; Negrete, C.A.; Dultzin, D.; Perea, J.; D'Onofrio, M. Highly Accreting Quasars at High Redshift. *Front. Astron. Space Sci.* **2018**, *4*, 65. [CrossRef]
69. Marziani, P.; Negrete, C.A.; Dultzin, D.; Martinez-Aldama, M.L.; Del Olmo, A.; Esparza, D.; Sulentic, J.W.; D'Onofrio, M.; Stirpe, G.M.; Bon, E.; et al. Highly accreting quasars: A tool for cosmology? *IAU Symp.* **2017**, *324*, 245–246. [CrossRef]
70. Marziani, P.; Sulentic, J.W. Quasars and their emission lines as cosmological probes. *Adv. Space Res.* **2014**, *54*, 1331–1340. [CrossRef]
71. Levi, M.; Bebek, C.; Beers, T.; Blum, R.; Cahn, R.; Eisenstein, D.; Flaugher, B.; Honscheid, K.; Kron, R.; Lahav, O.; et al. The DESI Experiment, a whitepaper for Snowmass 2013. *arXiv* **2013**, arXiv:1308.0847.
72. Shemmer, O.; Lieber, S. Weak Emission-line Quasars in the Context of a Modified Baldwin Effect. *Astrophys. J.* **2015**, *805*, 124. [CrossRef]
73. Jarvis, M.J.; McLure, R.J. Orientation dependency of broad-line widths in quasars and consequences for black hole mass estimation. *Mon. Not. R. Astron. Soc.* **2006**, *369*, 182–188. [CrossRef]
74. Marziani, P.; Olmo, A.; Martínez-Aldama, M.; Dultzin, D.; Negrete, A.; Bon, E.; Bon, N.; D'Onofrio, M. Quasar Black Hole Mass Estimates from High-Ionization Lines: Breaking a Taboo? *Atoms* **2017**, *5*, 33. [CrossRef]
75. Risaliti, G.; Lusso, E. A Hubble Diagram for Quasars. *Astrophys. J.* **2015**, *815*, 33. [CrossRef]